



LAWRENCE  
LIVERMORE  
NATIONAL  
LABORATORY

# Thermal drawdown-induced flow channeling in a single heterogeneous fracture in geothermal reservoir

B. Guo, P. Fu, Y. Hao, C. R. Carrigan

January 16, 2015

2015 Stanford Geothermal Workshop  
Stanford, CA, United States  
January 26, 2015 through January 28, 2015

## **Disclaimer**

---

This document was prepared as an account of work sponsored by an agency of the United States government. Neither the United States government nor Lawrence Livermore National Security, LLC, nor any of their employees makes any warranty, expressed or implied, or assumes any legal liability or responsibility for the accuracy, completeness, or usefulness of any information, apparatus, product, or process disclosed, or represents that its use would not infringe privately owned rights. Reference herein to any specific commercial product, process, or service by trade name, trademark, manufacturer, or otherwise does not necessarily constitute or imply its endorsement, recommendation, or favoring by the United States government or Lawrence Livermore National Security, LLC. The views and opinions of authors expressed herein do not necessarily state or reflect those of the United States government or Lawrence Livermore National Security, LLC, and shall not be used for advertising or product endorsement purposes.

# Thermal Drawdown-induced Flow Channeling in A Single Heterogeneous Fracture in Geothermal Reservoir

Bin Guo, Pengcheng Fu, Yue Hao, Charles R. Carrigan

Atmospheric, Earth, and Energy Division, Lawrence Livermore National Laboratory

P.O. Box 808, Livermore, CA 94551-0808

fu4@llnl.gov

**Keywords:** EGS, flow channeling, thermal drawdown, aperture heterogeneity, THM model

## ABSTRACT

In engineered geothermal systems, the spatial heterogeneity in fracture aperture plays an important role in flow pattern evolution, which significantly affects the reservoir performance. The initial flow field in a fracture is mainly determined by the aperture spatial distribution, and the pattern of the channeled flow tends to evolve due to the uneven temperature decrease during heat production. In geothermal reservoir either dominated by a single fracture or a fracture network, it is essential to understand the thermal drawdown-induced flow channeling in a single fracture with spatially heterogeneous aperture. In this study, we investigate the effects of aperture heterogeneity on flow pattern evolution in a single-fracture system. We especially focus on how the autocorrelation characteristics of the aperture field affect the reservoir production life, integrated production temperature, and average pressure loss. We use a discrete fracture network (DFN) -based numerical model to simulate the coupled thermal-hydrological-mechanical (THM) processes in a penny-shaped fracture intersecting with an injection well and a production well. Correlation length, ranging from 25 m to 150 m, is the primary independent variable under investigation, and a large number of realizations were performed to ensure the aperture spatial distributions are properly represented. We found that the correlation length does not affect the expectation of reservoir performance, while greater correlation lengths tends to increase the performance uncertainty. We also found that although the initial preferential path(s) always tend to carry a greater portion of flow over time, one or multiple preferential paths that deviate from the shortest line between the two wells can effectively improve the reservoir performance.

## 1. INTRODUCTION

A fundamental problem in the understanding of engineered geothermal systems (EGS) is the fluid flow pattern in a single fracture and the associated heat exchange between the working fluid and the surrounding rock medium, regardless whether the EGS is dominated by a single fracture (Baisch et al. 2006; Brown 1997; Brown and Duchane 1999; Brown 2009; Chopra and Wyborn 2003) or an interconnected fracture network (Drange 2011; Genter et al. 2012; Genter et al. 2013). It is highly desirable to have a diffusive flow pattern spreading over a large area of the fracture surface, as only the portion of the fracture that carries fluid flow provides effective heat exchange surface area. However, it is well known that fluid flow along a fracture in natural rock tends to be channelized along a few preferred pathways due to the inevitable spatial heterogeneity in the fracture aperture/transmissivity distribution (Tsang and Tsang 1989). Moreover, the pattern of channeled fluid flow is likely to evolve during EGS heat production. For instance, the flow channels that carry a higher flow rate might cool the surrounding rock faster. The cooler rock body can develop a greater thermal stress that reduces the effective stress and increases transmissivity of that portion of the fracture. This mechanism can potentially aggravate flow channeling by concentrating more flow in the portion of the fracture that is already cooled and reduce the heat production potential of EGS reservoirs.

The intrinsic spatial heterogeneity in fracture aperture plays the central role in the flow channeling phenomenon. Spatially heterogeneous fractures are widely observed in geologic formations (Kosakowski, Berkowitz, Scher 2001; Méheust and Schmittbuhl 2000; Neretnieks 1987), and the aperture spatial distribution of a single fracture affects both the initial flow pattern and the evolution of thermal drawdown-induced flow channeling during thermal production. The current study investigates the effects of the aperture heterogeneity on thermal drawdown-induced flow channeling in a single planar fracture in an EGS reservoir through fully coupled thermo-hydro-mechanical (THM) simulation. We especially focus on how the spatial autocorrelation characteristics of the aperture spatial distribution of the fracture affect the fate of heat production. A single fracture intersecting an injection well and a production well is simulated. The results are directly useful for EGS reservoirs that are dominated by a single fracture or a single fault zone (Baisch et al. 2006; Brown 1997; Brown and Duchane 1999; Chopra and Wyborn 2003), and they also provide insights into the behavior of individual fractures in a discrete fracture network.

## 2. COUPLED THM MODEL

### 2.1 Overview of the Model

We perform simulations using a discrete fracture network (DFN) -based numerical model, GEOS, developed at the Lawrence Livermore National Laboratory (Fu and Carrigan 2012; Settgest et al. 2012), to simulate the coupled THM processes in the heat production stage. Essential processes/mechanisms involved in the flow channeling phenomenon include:

1. Fluid flow along a fracture with a spatially autocorrelated aperture field;

2. Convective heat transfer associated with the fluid flow along the fracture, conductive heat transfer in the rock matrix, and heat exchange between the working fluid and the surrounding rock body;
3. The total stress change caused by the non-uniform cooling of the rock body; and
4. The evolution of the local fracture aperture as the effective stress changes.

The first two processes are simulated by a combined fracture-matrix flow solver in GEOS, as elaborated in Section 2.2. Thermal stress is calculated by a thermo-mechanical finite element solver and the total stress tensor of each rock matrix element is updated accordingly as briefly described in Section 2.3. Section 2.4 presents the procedure of updating the fracture aperture field based on temperature and stress change in the reservoir.

## 2.2 Flow and Heat Transfer in Fracture and Matrix

The flow and heat transfer solver combines fluid flow and heat transfer in both fractures and rock matrix in a unified finite element framework. Rock matrix is represented by 3D 8-node solid element and fractures, in the sense of their hydrological presence, are represented by planar 4-node elements. In this framework, a fracture flow element is set to be the shared face between the two solid elements that represent the rock body on the two sides of this fracture, and the four nodes are shared by these three elements. We use a node-based FEM formulation, and the independent state variables, namely temperature and fluid pressure, are solved for the nodes. In this way, the contributions from both the solid and fracture elements can be summed into the global system of governing equations in a natural and consistent manner.

Coupled single-phase flow and heat transfer in porous media are governed by the principle of mass conservation and energy conservation. The mass conservation equation for compressible fluid is

$$\frac{\partial(\rho\phi)}{\partial t} - \nabla(\rho\mathbf{v}) = \Gamma \quad (1)$$

where  $\rho$ ,  $\phi$ ,  $t$ ,  $\mathbf{v}$ , and  $\Gamma$  the fluid density, rock porosity, time, fluid velocity vector, and a source/sink term, respectively. According to Darcy's law, fluid velocity vector  $\mathbf{v}$  is calculated as

$$\mathbf{v} = \frac{\mathbf{k}}{\mu}(\nabla P - \rho g \nabla z) \quad (2)$$

where  $\mathbf{k}$ ,  $\mu$ ,  $P$ ,  $g$ , and  $z$  are the intrinsic permeability tensor of the rock matrix, fluid dynamic viscosity, fluid pressure, gravity acceleration, and depth, respectively. We assume the permeability of rock matrix is isotropic, so the permeability tensor is reduced to the permeability scalar  $k$ . Substituting Equation (2) into Equation (1) yields

$$\frac{\partial(\rho\phi)}{\partial t} - \nabla \left[ \rho \frac{k}{\mu} (\nabla P - \rho g \nabla z) \right] = \Gamma \quad (3)$$

The fluid density  $\rho$  depends on the pressure  $P$  and temperature  $T$ , and it is approximated by the following analytical function

$$\rho = \rho_r e^{[\beta_f(P-P_r) + \alpha_f(T-T_r)]} \quad (4)$$

where  $\rho_r$ ,  $P_r$ ,  $T_r$ ,  $\beta_f$ , and  $\alpha_f$  are the fluid density, pressure, temperature, fluid compressibility, and fluid thermal expansion coefficient in a known reference state, respectively. We assume that rock porosity  $\phi$  is a function of fluid pressure  $P$  as

$$\phi = \phi_r e^{\beta_r(P-P_r)} \quad (5)$$

where  $\phi_r$  and  $\beta_r$  are the rock porosity and rock compressibility in a reference state, respectively. The permeability of rock matrix is associated with porosity and their relationship is described with the following power law

$$k = k_0 \left( \frac{\phi}{\phi_0} \right)^n \quad (6)$$

where  $k$ ,  $k_0$ ,  $\phi_0$ , and  $n$  are the current permeability, initial permeability, initial porosity, and an empirical power index of the rock matrix, respectively.

For a non-isothermal system, we have energy balance over both the fluid phase and the solid phase in a porous medium, and the governing equation is

$$\frac{\partial}{\partial t} (\phi \rho C_f T + (1 - \phi) \rho_s C_s T) + \nabla (\rho C_f T v) = \nabla (K_m \nabla T) + Q \quad (7)$$

where  $C_f$ ,  $\rho_s$ ,  $C_s$ ,  $K_m$ , and  $Q$  are the fluid heat capacity, rock solid density, solid heat capacity, thermal conductivity of rock matrix, and a source/sink term, respectively. These are the equations used in our generic matrix and fracture flow solver. Note that for the EGS scenarios investigated in the current study, the fluid flow in the rock matrix, although exists, plays a minimal role, and so does the porosity change dictated by equation (6).

Equation (3) and Equation (7) also apply to fractures as long as we use a unity porosity for the fracture elements and use

$$k = \frac{A^2}{12} \quad (8)$$

to calculate the equivalent permeability of the fracture element, where  $A$  is fracture aperture.

We use an implicit time integration scheme in the flow solver and the time step size is adaptively adjusted. Generally, small time steps are required in the beginning of the heat production due to the high degree of transience of the system. As the system evolves into a semi-steady state, the solution can remain stable even if a relatively long time step is used. Because we have to update the thermal stress and the fracture aperture field between adjacent time steps of the flow solver, we limit the time step size to be no longer than one month. We found that further reducing this maximum time step size does not alter the simulation results, implying satisfactory numerical convergence.

### 2.3 Calculation of Thermal Stress

Because the fracture remains mechanically closed (but hydraulically permeable) under the high *in situ* compressive stress, we treat the rock body containing the closed fracture as a continuum for the calculation of thermal stress. The finite element mesh for the solid thermo-mechanical solver is the same as the solid mesh for the flow solver except that the planar flow elements in the latter are not included. We map the node-based temperature field obtained by the flow solver onto the continuum FEM mesh. The thermal stress field is obtained following the procedure outlined in Section 2.10 of Cook et al. (2007). The approach is a standard method employed in thermo-mechanical finite element analysis and not repeated here.

### 2.4 Updating the Fracture Aperture Field

Three types of information are required to update the fracture aperture during the simulation of the heat production: 1) total stress normal to the fracture plane, 2) the fluid pressure field in the fracture, and 3) a rock joint model. The total stress tensor of the rock body, including the contributions of the far-field *in situ* stress and the thermal stress, is a direct output of the thermo-mechanical FEM solver. For each fracture element, we calculate the total normal stress based on the average of the stress tensors in the two adjacent solid elements. The fluid pressure in each fracture element is obtained from the flow solver, and the difference between the total normal stress and the fluid pressure is the effective normal stress  $\sigma'_n$  of the fracture element. We assume that the aperture of each fracture element is solely determined by the effective normal stress on this element and not affected by the stress state of the adjacent fracture elements, and use the classic Barton-Bandis model (Bandis, Lumsden, Barton 1983; Barton, Bandis, Bakhtar 1985) to calculate the aperture.

The Barton-Bandis model for rock joints has been widely used in various numerical models for fracture-dominated geothermal reservoirs (Bower and Zyvoloski 1997; Bruel 2002; Kohl et al. 1995). We rewrite the original equation to express aperture as a function of effective stress as following

$$A = A_{\max} - \frac{a \sigma'_n}{1 + b \sigma'_n} \quad (9)$$

where  $A$  and  $A_{\max}$  are the aperture under the current effective normal stress  $\sigma'_n$  and aperture at zero (or minimal) effective stress, respectively.  $a$  and  $b$  are two material- and state-dependent parameters. We assume that the aperture approaches zero as the effective stress approaches infinity so that the relationship of  $A_{\max} = a/b$  reduces the independent parameters to  $a$  and  $b$  alone. Essentially, the random field of fracture aperture (including its current state and its deformation characteristics) can be represented by a field of parameter  $a$  and a field of parameter  $b$ . However, the study of the spatial distribution of aperture in the literature has been directly quantifying the aperture itself, but not these two parameters. To make the random generation of the aperture field more straightforward, we adopt the apertures  $A_{r1}$  and  $A_{r2}$  in two known reference stress states  $\sigma'_{n,r1}$  and  $\sigma'_{n,r2}$  as an alternative set of independent parameters. Through the following relationship between these two sets of parameters

$$a = \frac{A_{r1}(A_{r1} - A_{r2})}{\sigma_{r2} A_{r2}} \quad (10)$$

$$b = \frac{A_{r1} - A_{r2}}{\sigma_{r2} A_{r2}} \quad (11)$$

we can generate two random aperture fields in two pre-specified stress states, and obtain the fields of  $a$  and  $b$  indirectly.

### 3. SETUP OF THE MODEL

#### 3.1 The Simulation Domain

We simulate the heat production from a horizontal penny-shaped fracture in a large body of low-permeability hot rock. The diameter of the fracture is 1,000 m, with a depth of 2,000 m. One injection well and one production well are connected to the fracture and the distance between the two wells is 500 m. Figure 1 shows the system configuration as well as the three principal components of the *in situ* stress. Because the site is in a reverse faulting region with the vertical stress being the minimum principal component, the horizontal fracture can be an engineered fracture or a natural fracture (Baisch et al. 2006; Baisch et al. 2009; Chopra and Wyborn 2003). During the simulated heat production stage, we ensure that the fluid pressure never exceeds the minimum principal stress, so the size of the fracture is fixed. The initial pore pressure is 22 MPa, and the initial reservoir temperature is 200 °C (392 °F).

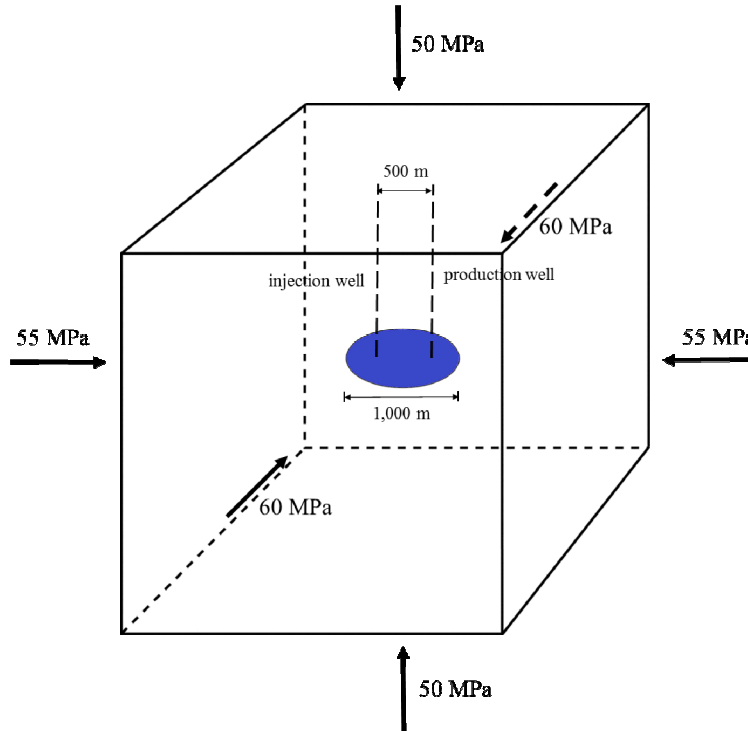


**Figure 1: Model system and *in situ* stress**

The size of the simulation domain is approximately  $3 \text{ km} \times 3 \text{ km} \times 3 \text{ km}$ , much larger than the volume affected by heat transfer, to simulate the constraints of the far-field rock body in thermal stress development. Near the fracture, the mesh resolution is 10 m in the  $x$ - and  $y$ -directions and 5 m in the  $z$ -direction. The mesh becomes progressively coarser at locations farther from the fracture to reduce the computational cost. The computational domain consists of 875,000 solid elements.

The downhole pressure in the production well at the depth of the fracture is 22 MPa and we fix the injection rate of 20 kg/s at the injection well. The temperature of the injected water remains at 50 °C (122 °F) throughout the operation. We apply a zero-flow boundary condition at the far-field boundaries. Due to the very low permeability of the rock matrix, the fracture is essentially a closed-loop flow system, and the production rate quickly reaches and stabilizes at 20 kg/s. The thermo-mechanical FEM solver applies the “roller” boundary condition on one boundary face in each direction and apply the specified *in situ* stress on the opposite boundary face in the same direction, which is a typical way of applying *in situ* stress while eliminating the rigid body motion of the model.

Except for the parameters of the rock joint model, the rest of the parameters used in the model are shown in Table 1.

**Table 1: Rock properties, fluid properties, and other parameters used in the model**

Property Name	Symbol	Units	Value
Initial permeability of rock matrix	$k_0$	$\text{m}^2$	$1 \times 10^{-22}$
Reference porosity of rock matrix	$\square_r$	—	$1 \times 10^{-4}$
Initial porosity of rock matrix	$\square_0$	—	$1 \times 10^{-4}$
Rock compressibility	$\beta_r$	$\text{Pa}^{-1}$	$4.0 \times 10^{-10}$
Rock solid density	$\rho_s$	$\text{kg}/\text{m}^3$	2700
Rock solid heat capacity	$C_s$	$\text{J}/\text{kg}/\text{K}$	790
Thermal conductivity of rock matrix	$K_m$	$\text{W}/\text{m}/\text{K}$	2.9
Rock bulk modulus	$K$	GPa	50
Rock shear modulus	$G$	GPa	35
Fluid dynamic viscosity	$\mu$	$\text{Pa s}$	$1.507 \times 10^{-4}$
Reference fluid density	$\rho_r$	$\text{kg}/\text{m}^3$	898.31
Fluid compressibility	$\beta_f$	$\text{Pa}^{-1}$	$4.497 \times 10^{-10}$
Fluid thermal expansion coefficient	$\alpha_f$	$\text{K}^{-1}$	$7.07 \times 10^{-4}$
Fluid heat capacity	$C_f$	$\text{J}/\text{kg}/\text{K}$	$4.318 \times 10^{-3}$
Reference pressure	$P_r$	MPa	22
Reference temperature	$T_r$	$^{\circ}\text{C}$	200
Empirical power index	$n$	—	3

### 3.2 The generation of the heterogeneous aperture field

The aperture field of the fracture is an essential component of our numerical model. It is known to be a spatially autocorrelated random field (Tsang and Neretnieks 1998; Tsang et al. 1988; Tsang and Tsang 1989) and it can be mathematically quantified by the probability distribution of the aperture, the correlation length, and the variogram. In a given stress state, the aperture has been found to typically follow the gamma distribution or the lognormal distribution (Tsang and Neretnieks 1998; Tsang et al. 1988; Tsang and Tsang 1989). As described in section 2.4, we need to generate two fracture aperture fields corresponding to two given stress states to fully quantify the deformation characteristics of the fracture. We choose the initial natural state (28 MPa effective normal stress) as the first reference state and for this state we adopt the aperture data from Tsang et al. (1988), which follow a lognormal distribution with a mean aperture of 0.24 mm and a standard deviation of 0.17 mm. We cut the “long tail” of the lognormal distribution of the aperture at the maximum aperture of 0.6 mm. We choose the effective stress of 1 MPa as the second reference state and assume that the aperture in this state is three times of that in state 1. This seemingly arbitrary choice of the correlation between the apertures in these two states reflects the unfortunate lack of real data. However, it is sufficient to embody the most essential behavior of rock joints concerned in this study: fracture aperture and transmissivity increase significantly as the effective stress decreases. We use the same probability distribution of apertures for all the simulations in the current paper, and the correlation length is the primary variable we investigate.

The spatial autocorrelation of aperture is described by the correlation length  $\lambda$  and the variogram. The  $\lambda/L$  ratio, with  $L$  being the characteristic flow length, is between 0.05 and 0.30 for typical hydrological applications (Tsang and Neretnieks 1998; Tsang et al. 1988; Tsang and Tsang 1989). In our single fracture two-well system, the characteristic flow length  $L$  is the distance, 500 m, between the two wells. Therefore, we use six values of  $\lambda$ , namely 25 m, 50 m, 75 m, 100 m, 125 m, and 150 m in our study. The exponential, spherical, and Gaussian variogram models are widely used in geostatistics (Chiles and Delfiner 2009; Cressie 1993) while the variogram curves of the three forms only differ slightly. We use the exponential variogram model in the present study, and the effects of the variogram model choice is minimal.

To obtain statistically sound results, we need to generate a sufficiently large number of random realizations for each set of specified parameters. We use the frequentist method described in Adcock (1997) and Desu (2012) to determine the minimum number of realizations required. The results show that between 10 and 25 realizations are needed for each correlation length level, with the longer correlation length requiring more random realization. The numbers of realizations included in the current study are 16, 27, 32, 36, 41, and 43, respectively for the six levels of  $\lambda$ , much more than the minimum required numbers. We use R, a programming language for statistical computing and graphics, to generate the aperture fields that follows the aforementioned probability distribution in the initial state (28 MPa effective stress).

## 4. SIMULATION RESULTS

### 4.1 Observations on A Representative Case

First, we use the results of one representative case to illustrate the HTM processes observed in the numerical models. Figure 2 shows the results of a realization of  $\lambda=100$  m, and the results include the evolution of aperture field and temperature field of the fracture, the production temperature curve, and the injection pressure over 30 years of heat production.

We can identify two preferred flow paths between the two wells as denoted by the two dash-dotted lines in the 3-month snapshot of the aperture field. The two paths are related to the portions of the relatively wide fracture. Due to the small aperture near the center of the fracture, these two preferred flow paths are on the upper and lower parts of the fracture, respectively, in a tortuous manner. The rock body along these two paths cools faster than the other portions, and we can observe that the apertures along these paths further increase due to the mechanism that we described in section 1. Eventually, the lower preferred path gains dominance over the upper path, and the two wells are connected by this path throughout. During this process, the production temperature continuously decreases following the thermal breakthrough as early as year 1. Meanwhile, the pressure drop between the two wells also decreases due to the increasing aperture along the preferred flow path(s). This example evidently demonstrates that our THM numerical model adequately capture the flow channeling mechanism described in section 1.

To make the subsequent statistical analysis of the hundreds of simulations tractable, we define the following three metrics that represent the essential characteristics of the EGS in a concise manner. 1) The **production life** is defined as the time period when the production temperature continuously drops from the initial 200°C to 100°C. The value of lower temperature fluid for electricity generation is minimal. In the example above, the production life (17.8 years) is determined from the production temperature decline curve. 2) The **production temperature integral** is defined as the area between the production temperature history curve and the horizontal line of 100°C temperature, as illustrated by the shaded area in Figure 2. This metric quantify the useable heat produced by the EGS. 3) The **average pressure loss** is defined as the difference between the downhole pressures in the two wells at the fracture depth. It affects the pumping power consumed to drive the EGS.

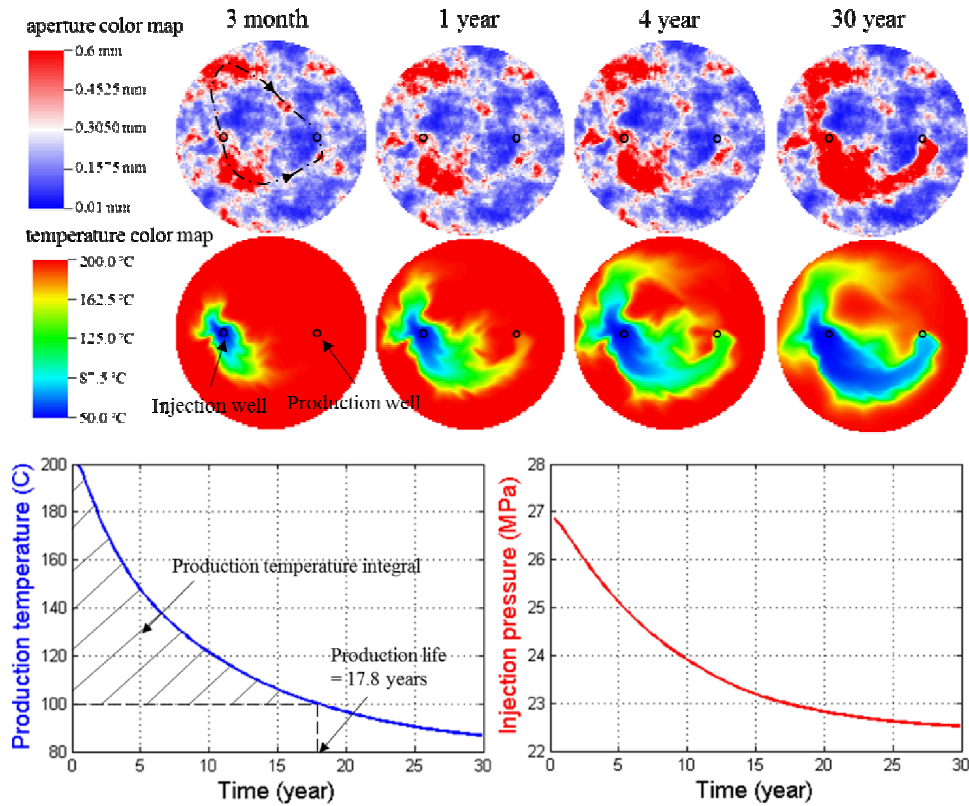


**Figure 2: Aperture field, temperature field, production temperature, and injection pressure for one simulation example with correlation length of 100 m**

### 4.2 Statistical Analysis of All Cases

The scatter plots of the three metrics, namely the production life, the production temperature integral, and the average pressure loss as functions of the correlation length  $\lambda$  of the random aperture field, are shown in Figure 3(a), (b), and (c), respectively for all the cases simulated. The mean values and the standard deviations of these metrics calculated based on all the random realizations of each correlation length level are summarized in Table 2. The results show that the  $\lambda$  value only has a minimal effect on the mean values of all the metrics. Considering the high variance, this effect is not statistically significant. The effects of the  $\lambda$  value on the standard deviation of each metric are more significant, and the effects are also quite consistent among the three metrics. A longer correlation length

generally results in greater variance in either metric. The correlation length essentially quantifies the dimensions of the high/low permeability “patches”. A small  $\lambda$  value means the high/low permeability patches are small and calculated metrics reflect the sufficiently homogenized effects of these patches on EGS behavior. As the correlation length increases, these high/low aperture patches become larger and a small number of such large patches can determine the EGS’s behavior, resulting in greater variances. Moreover, the variance seems to “saturate” at certain  $\lambda$  value and it oscillates slightly as we further increase the  $\lambda$  value. The threshold  $\lambda$  values for the production life, production temperature integral, and average pressure loss are 50 m, 100 m, and 100 m respectively.

**Table 2: Means and standard deviations of production life, production temperature integral, and average pressure loss**

Correlation length		25 m	50 m	75 m	100 m	125 m	150 m
Production life (year)	mean	19.6	20.8	19.9	19.2	20.4	21.0
	standard deviation	5.8	7.6	8.0	8.5	7.5	7.8
Production temperature integral (°C*year)	mean	546.8	636.9	605.0	608.8	623.5	704.9
	standard deviation	153.2	289.8	339.4	380.7	302.6	396.0
Average pressure drop (MPa)	mean	1.19	1.92	1.60	2.42	2.39	1.68
	standard deviation	0.56	1.19	1.60	2.18	2.27	1.29

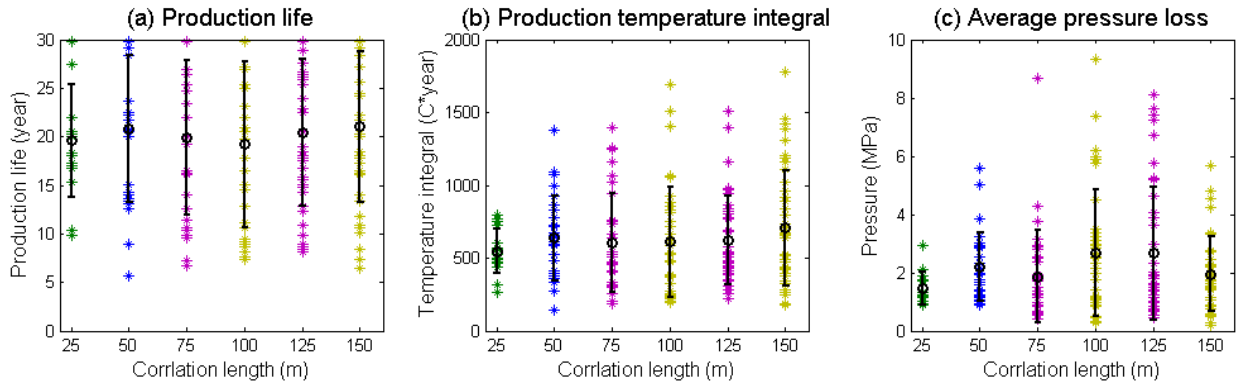


**Figure 3: Scatter plots of (a) production life, (b) production temperature integral, and (c) average pressure loss, marked with mean and standard deviation**

#### 4.3 The Relationship between Flow Pattern and EGS Performance

The results in the previous section show that EGS performance varies over a great range depending on the random realizations of the specified statistical characteristics of the aperture field. For instance, for the correlation length  $\lambda$  of 50 m, the shortest effective production life is 5.7 years and there are 7 among the 27 realizations obtaining production lives exceeding 30 years. In this section, we investigate the aperture spatial distribution features that determine the EGS performance.

To this end, we use the correlation lengths of 50 m and 125 m as examples and pick four realizations that covering a wide range of performance for each  $\lambda$  value. We visualize the evolution of the aperture field and fracture temperature field of these eight realizations in Figure 4 and Figure 5. These cases show the common behaviors that we have observed in the representative case described in detail in section 4.1. We observe that if the initial aperture field enables a low hydraulic impedance flow path that directly connects the wells with a relatively straight line to form, flow tends to further channelize into this direct and short path, causing quick thermal breakthrough and fast thermal drawdown. On the contrary, some initial aperture fields force highly tortuous flow paths, particularly multiple paths remarkably deviate from the straight line connecting the two wells to form. Although the flow does tend to eventually channelize in one dominant path, we still obtain superb EGS performance due to the large heat exchange surface area associated with these flow patterns. The realizations with the aperture fields in the latter category usually have a large low permeability patch at the center area of the fracture.

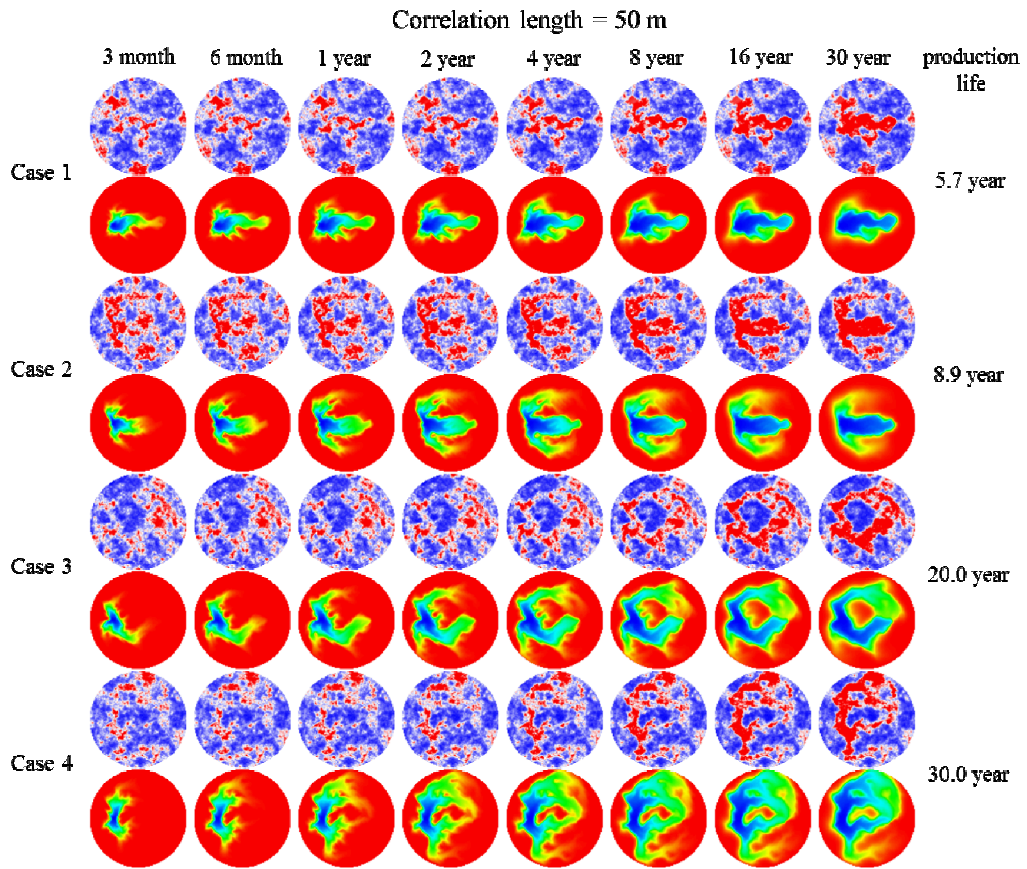
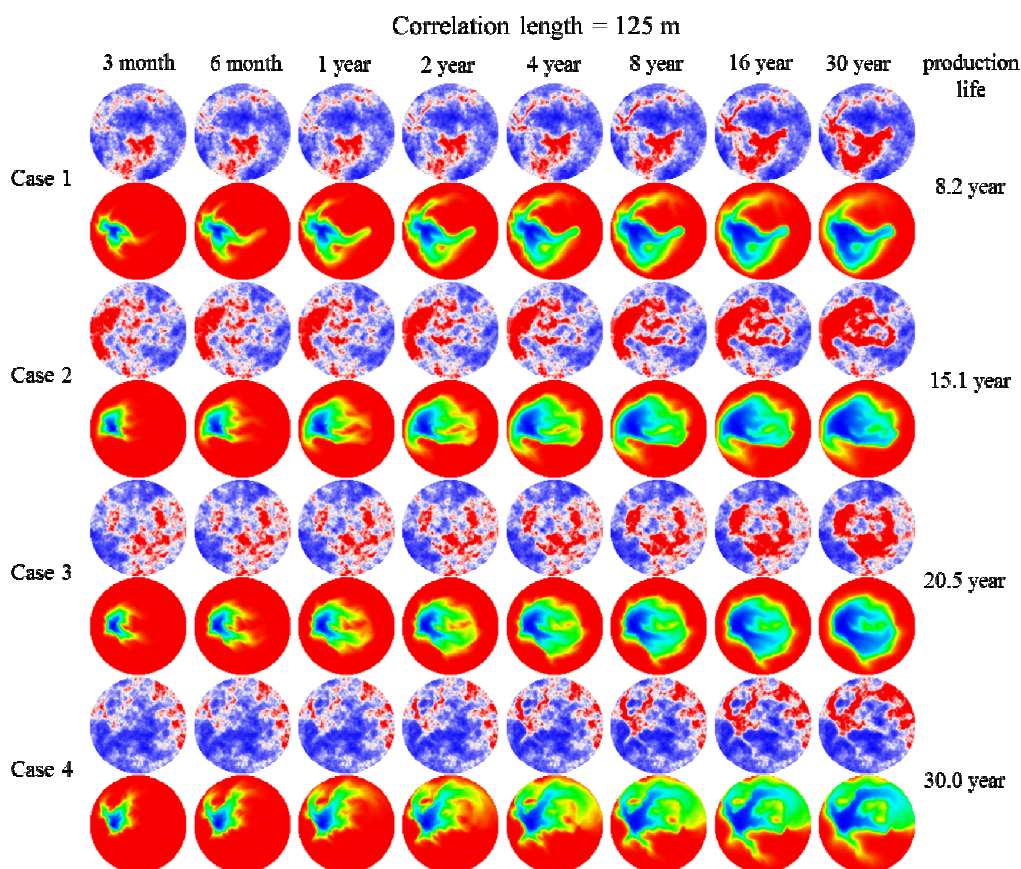


Figure 4: Snapshots of various aperture evolutions and temperature fields for correlation length of 50 m (the color maps are the same with those in Figure 2)



**Figure 5: Snapshots of various aperture evolutions and temperature fields for correlation length of 150 m (the color maps are the same with those in Figure 2)**

## 5. CONCLUSIONS

We developed a fully coupled Thermo-Hydro-Mechanical numerical model to capture the flow channeling process on a single fracture in EGS reservoir. Using this tool, we primarily studied the effects of the spatial correlation length of the fracture aperture field on EGS performance. A large number of random realizations were generated to ensure the spatially heterogeneous fracture is statistically represented. We found that the correlation length, which describes the spatial autocorrelation characteristics, does not affect the mean or expected performance of the EGS, whereas greater correlation lengths tend to increase the variance of the heat production performance. These two aspects of EGS performance have direct implications for the overall total performance of a large reservoir consisting of multiple injection-production duplets and the uncertainties in heat production and maintenance cost, respectively. We also found that although the fate of flow channeling is inevitable regardless of the initial flow pattern, the EGS tends to have long-lasting heat production if the initial aperture field generates one or multiple preferential flow paths that deviate from the short and direct path between the two wells.

## Acknowledgement

The authors gratefully acknowledge the Geothermal Technologies Program of the US Department of Energy for support of this work under the Enhanced Geothermal Systems Program. The authors also would like to acknowledge their collaborators at the Lawrence Livermore National Laboratory. This work was performed under the auspices of the U.S. Department of Energy by Lawrence Livermore National Laboratory under Contract DE-AC52-07NA27344.

Release number: LLNL-PROC-666271.

## REFERENCES

- Adcock, C.J.: Sample Size Determination: A Review, *Journal of the Royal Statistical Society: Series D (The Statistician)*, **46.2**, (1997), 261-83.
- Baisch, S. et al.: Investigation of Fault Mechanisms during Geothermal Reservoir Stimulation Experiments in the Cooper Basin, Australia, *Bulletin of the Seismological Society of America*, **99.1**, (2009), 148-58.
- Baisch, S. et al.: Induced Seismicity during the Stimulation of a Geothermal HFR Reservoir in the Cooper Basin, Australia, *Bulletin of the Seismological Society of America*, **96.6**, (2006), 2242-56.

- Bandis, S.C., Lumsden A.C., and Barton N.R.: Fundamentals of Rock Joint Deformation, *International Journal of Rock Mechanics and Mining Sciences & Geomechanics Abstracts*, Elsevier, (1983), 249-268.
- Barton, N., Bandis S., and Bakhtar K.: Strength, Deformation and Conductivity Coupling of Rock Joints, *International Journal of Rock Mechanics and Mining Sciences & Geomechanics Abstracts*, Elsevier, (1985), 121-140.
- Bower, K.M., and Zyvoloski G.: A Numerical Model for Thermo-Hydro-Mechanical Coupling in Fractured Rock, *International Journal of Rock Mechanics and Mining Sciences*, **34.8**, (1997), 1201-11.
- Brown, D. Review of Fenton Hill HDR test results, (1997).
- Brown, D.W., and David V.D.: Scientific Progress on the Fenton Hill HDR Project since 1983, *Geothermics*, **28.4**, (1999), 591-601.
- Brown, Donald W.: Hot Dry Rock Geothermal Energy, Important Lessons from Fenton Hill". *Proceedings*, 34th Workshop on Geothermal Reservoir Engineering, Stanford University, CA (2009).
- Bruel, D.: Impact of Induced Thermal Stresses during Circulation Tests in an Engineered Fractured Geothermal Reservoir, Example of the Soultz-Sous-Forets European Hot Fractured Rock Geothermal Project, Rhine Graben, France, *Oil & Gas Science and Technology*, **57.5**, (2002), 459-70.
- Chiles, J., and Pierre D.: *Geostatistics, Modeling Spatial Uncertainty*. 497 Vol. John Wiley & Sons, (2009).
- Chopra, P., and Doone W.: Australia's First Hot Dry Rock Geothermal Energy Extraction Project is Up and Running in Granite Beneath the Cooper Basin, NE South Australia, *Proceedings*, Ishihara Symposium, Granites and Associated Metallogeneses, (2003), 43-45.
- Cook, R.D.: Concepts and Applications of Finite Element Analysis. John Wiley & Sons, (2007).
- Cressie, N.: Statistics for Spatial Data, Wiley Series in Probability and Statistics, (1993).
- Desu, M.M.: Sample Size Methodology. Elsevier, (2012).
- Drange, L.A.: Engineered Geothermal Systems, (2011).
- Fu, P., and Carrigan C.R.: Modeling Responses of Naturally Fractured Geothermal Reservoir to Low-Pressure Stimulation, *The 36th Annual Meeting of Geothermal Resources Council*, (2012).
- Genter, A. et al.: Status of the Soultz Geothermal Project during Exploitation between 2010 and 2012, *Proceedings*, 37th Workshop on Geothermal Reservoir Engineering, Stanford University, CA (2012).
- Genter, A., et al.: Main Achievements from the Multi-Well EGS Soultz Project during Geothermal Exploitation from 2010 and 2012, *Proceedings*, European Geothermal Energy Congress, EGC 2013, (2013).
- Kohl, T., et al.: Coupled Hydraulic, Thermal and Mechanical Considerations for the Simulation of Hot Dry Rock Reservoirs, *Geothermics*, **24.3**, (1995), 345-59.
- Kosakowski, G., Berkowitz B., and Scher H.: Analysis of Field Observations of Tracer Transport in a Fractured Till, *Journal of contaminant hydrology*, **47.1**, (2001), 29-51.
- Méheust, Y., and Schmittbuhl J.: Flow Enhancement of a Rough Fracture, *Geophysical Research Letters*, **27.18**, (2000), 2989-92.
- Neretnieks, I.: Channeling Effects in Flow and Transport in Fractured rocks—Some Recent Observations and Models, *Proceedings*, GEOVAL-87, International Symposium, Stockholm, Sweden (1987), 315-335.
- Settgast, R., et al.: Simulation of Hydraulic Fracture Networks in Three Dimensions, *Proceedings*, 37th Stanford Geothermal Workshop, Stanford University, CA (2012).
- Tsang, C.F., and Neretnieks I.: Flow Channeling in Heterogeneous Fractured Rocks, *Reviews of Geophysics*, **36.2**, (1998), 275-98.
- Tsang, Y.W., et al.: Flow and Tracer Transport in Fractured Media, A Variable Aperture Channel Model and its Properties, *Water Resources Research*, **24.12**, (1988), 2049-60.
- Tsang, Y.W., and Tsang C.F.: Flow Channeling in a Single Fracture as a two-dimensional Strongly Heterogeneous Permeable Medium, *Water Resources Research*, **25.9**, (1989), 2076-80.